Front. Phys. 13(5), 137107 (2018)
https://doi.org/10.1007/s11467-018-0818-7

RESEARCH ARTICLE

Pressure-induced superconducting ternary hydride H_3SXe: A theoretical investigation

Da Li (李达), **Yan Liu** (刘妍), **Fu-Bo Tian** (田夫波), **Shu-Li Wei** (魏书丽), **Zhao Liu** (刘召), **De-Fang Duan** (段德芳), **Bing-Bing Liu** (刘冰冰), **Tian Cui** (崔田)†

State Key Lab of Superhard Materials, College of Physics, Jilin University, Changchun 130012, China
Corresponding author. E-mail: †cuitian@jlu.edu.cn
Received March 10, 2018; accepted May 30, 2018

In general, heavy elements contribute only to acoustic phonon modes, which are less important for the superconductivity of hydrides. However, it was revealed that the heavier elements could enhance the phonon-mediated superconductivity in ternary hydrides. In the H_3S–Xe system, a novel H_3SXe compound was discovered by first-principle calculations. The structural phase transitions of H_3SXe under high pressures were studied. The R-3m phase of H_3SXe was predicted to appear at pressures above 80 GPa, which transitions to $C2/m$, P-3m1, and Pm-3m phases at pressures of 90, 160, and 220 GPa, respectively. It has been anticipated that the Pm-3m-H_3SXe phase with a similar structural feature as that of Im-3m-H_3S is a potential high-temperature superconductor with a T_c of 89 K at 240 GPa. The T_c value of H_3SXe is lower than that of H_3S at high pressure. The "H_3S" host lattice of Pm-3m-H_3SXe is a crucial factor influencing the T_c value. The Xe atoms could accelerate the hydrogen-bond symmetrization. With the increase of the atomic number, the T_c value linearly increases in the H_3S–noble-gas-element system. This indicates that the superconductivity can be modulated by changing the relative atomic mass of the noble-gas element.

Keywords ternary hydrides, noble gas elements, chemical precompression, hydrogen-bond symmetrization

PACS numbers 71.10.-w, 71.15.Mb, 74.25.Dw, 61.50.Ah

1 Introduction

Recently, the superconductivity of the H_2S sample under high pressure has attached much attention [1, 2]. The high superconducting critical temperature T_c (190 K) of the H_2S sample above 150 GPa has been observed by using the electrical resistance, magnetic susceptibility and magnetization measurements in experiments [3]. Previous experiments suggest that the H_2S decomposes under high pressure to the pure sulfur and hydrogen-rich sulfur hydride [4]. Our previously predicted Im-3m-H_3S was seen as the candidate crystal structure of the above mentioned high-pressure superconducting hydrogen-rich sulfur hydride [5]. The Im-3m phase of H_3S has a similar superconducting critical temperature–pressure relationship as the observation in experiments. Subsequent, the x-ray diffraction and electrical resistance measurements confirm that the experimentally observed superconducting phase is in good agreement with our theoretically predicted body-centered cubic Im-3m H_3S phase [4]. Up to now, many excellent studies about the Im-3m phase of H_3S were performed by using different methods [6–18]. The effect of the nonempirical electron-electron coulomb interaction, anharmonic effect, ionic character, and the exchange correlation effects have been seriously considered in the study of H_3S [19–24]. However, there are still some debate in the superconductivity of high-pressure H_2S sample. Very recently, Goncharov *et al.* confirmed that the presence of Im-3m H_3S in their synchrotron X-ray diffraction and Raman spectroscopy experiment [25]. But similar experiment performed by Guigue *et al.* indicates that the Im-3m H_3S is absence above 140 GPa [26]. More studies in the superconductivity of high-pressure H_2S are needed. In addition to the well-known H_3S, many other hydrogen-rich compounds have also been proposed such as CaH_6, LaH_{10}, YH_{10}, UH_7, H_3P, H_xS_y, H_xSe_y, H_4Te, H_5Te_2, BiH_x, SbH_4, and

*Dedicated to Prof. Guangtian Zou on the occasion of his 80th birthday.

AsH_8 [27–42]. Recently, Hoffmann *et al.* suggest that the ternary gold hydrides are potentially superconducting compounds at lower pressures. The high-pressure $KAuH_2$ is predicted to be a superconductor with the T_c of 0.3 K. The $Ba(AuH_2)_2$ and $Sr(AuH_2)_2$ are predicted to be stable at pressure of 1 atm. However, their superconducting critical temperature are only 30 and 10 K, respectively [43]. Zhang *et al.* predicted an orthorhombic Fe_2SH_3 with the electron phonon coupling parameter of 0.3 and T_c value of 0.3 K at 173 GPa [44]. Earlier experiments suggest that the hydrogen-rich ternary $BeReH_9$ transforms into a metal and then a superconductor above 100 GPa. However, its maximum superconducting critical temperature is only 7 K [45]. Up to now, many ternary hydrides have been studied [46, 47]. Although their T_c value is not very high, they give us a new route to find high-temperature superconductors. Therefore, it is desirable to investigate the properties of ternary hydrides with different dopants. It is found that the dopant can reduce the synthesis pressure of hydrogen-rich hydrides. However, many fundamental aspects are not well understood. Specifically, the relationship between dopant and superconductivity are still far from being clear. Moreover, there are little study about the noble gas elements doped hydrides.

In this paper, we aim to study the effect of chemical precompression on H_3S, induced by doping the noble gas elements, using the first principle methods. Due to good chemical inert properties and bigger atomic mass and radius, xenon is the most promising noble gas element. We investigate whether or not the xenon atoms can decrease the synthesis pressure of H_3S and enhance the degree of hydrogen-bond symmetrization of H_3S. The results show that there are novel H_3SXe compounds composed of noble gas element Xe and H_3S at lower pressures. The high-pressure phase transitions have been studied. The Xe atoms have the capability to accelerate the hydrogen-bond symmetrization in H_3SXe. However, although the high-pressure H_3SXe with *Pm*-3*m* space group has similar structural parameters as that of *Im*-3*m* H_3S, the T_c of *Pm*-3*m*-H_3SXe (89 K @ 240 GPa) is lower than that of *Im*-3*m* H_3S (200 K @ 200 GPa). Furthermore, the relationship between atomic mass and dopant-induced superconductivity is revealed.

2 Computational methods

Most calculations are performed within the density functional theory (DFT) [48, 49], carried out within the Vienna *ab initio* simulation package (VASP), with the projector augmented wave method [50–52]. The H $1s^1$, S $3s^23p^4$ and Xe $5s^25p^6$ electrons are treated as valence electrons, respectively. The Perdew–Burke–Ernzerhof generalized gradient approximation (GGA) exchange and correlation functional (H_GW, S_GW, and Xe_GW pseudopotential) are used [53]. Convergence tests give a kinetic energy cutoff 800 eV, with a grid of spacing $2\pi \times 0.03$ Å^{-1} for the electronic Brillouin zone (BZ) integration in all phases. The geometries are optimized when the remanent Hellmann–Feynman forces on the ions are less than 0.01 eV/Å. The heat of formation (ΔH_f) for H_3S-Xe system are calculated by the equation of $\Delta H_f = E_{\text{total}}[(H_3S)_xXe_y] - (xE_{\text{total}}(H_3S) + yE_{\text{total}}(Xe))$. And the *Cccm* (stable at 37 GPa–111 GPa), *R*3*m* (stable at 111 GPa–180 GPa), *Im*-3*m* (stable above 180 GPa) phases of H_3S and *hcp* phase of Xe are adopted. The phonon frequencies are calculated by using a supercell approach as implemented in the PHONOPY code with $3 \times 3 \times 3$ supercell [54]. The forces are calculated from VASP code. The calculation of the electron-phonon coupling (EPC) parameter λ are performed using the pseudopotential plane-wave method within the density functional perturbation theory as implemented in the Quantum-ESPRESSO code [55]. The generalized gradient approximation correction (GGA) of PBE within norm-conserving pseudopotentials of Martins-Troullier form was tested to be used. The kinetic energy cutoff and the charge density cutoff of the plane wave basis were chosen to be 80 and 320 Ry, respectively. A $6 \times 6 \times 6$ *q*-point mesh in the first Brillouin zone is used in the EPC calculation. A grid of $24 \times 24 \times 24$ is used to ensure *k*-point. A Gaussian broadening of 0.03 is used to calculate the phonon linewidth.

3 Results and discussion

In order to study the chemical precompression induced by Xe atoms, the extensive structural searches on H–S–Xe compounds for various stoichiometry of $H_xS_yXe_z$ (x, y, z = 0–1) at selected pressures of 0, 30, 80, 150, 200, and 300 GPa are performed by using the CALYPSO code [56, 57]. The candidate structures for each composition are then used to evaluate heat of formation (ΔH_f) relative to H_3S and Xe. By evaluating the averaged ΔH_f for each composition at 0 K and different pressures, the convex hull data for H_3S–Xe system at different pressures are obtained (Fig. S1). It is found that only one stable stoichiometry 3:1:1 (H_3SXe) appears in the pressure range of 0–300 GPa. Four novel H_3SXe compounds with *R*-3*m*, *C*2/m, *P*-3*m*1 and *Pm*-3*m* space groups (hereafter denoted as *R*-3*m*-H_3SXe, *C*2/m-H_3SXe, *P*-3*m*1-H_3SXe and *Pm*-3*m*-H_3SXe) are found in our calculations. The simulated enthalpy *vs* pressure curves indicate that *R*-3*m*-H_3SXe is more energetically favorable than H_3S and Xe at pressures above 80 GPa (Fig. 1). At 90 GPa, *R*-3*m*-H_3SXe predictably undergoes a hexagonal *R*-3*m* → monoclinic *C*2/m phase transition. The *C*2/m-H_3SXe transforms to *P*-3*m*1 phase at 160 GPa.

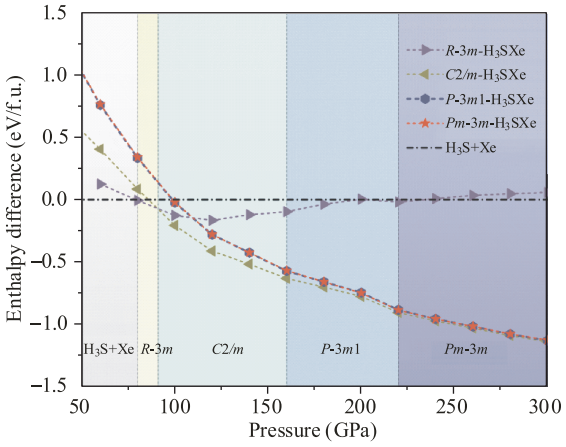

Fig. 1 Enthalpy difference curves of H_3SXe.

Then the P-3m1-H_3SXe phase transforms to cubic Pm-3m-H_3SXe at 220 GPa. We calculated the phonon density curves of these four H_3SXe compounds within a wide pressure range up to 300 GPa. No imaginary frequencies are observed throughout the whole Brillouin zone, confirming dynamical stability of R-3m-H_3SXe, $C2/m$-H_3SXe, P-3m1-H_3SXe, and Pm-3m-H_3SXe (Fig. S2). The novel H_3SXe compounds are stable at pressures above 80 GPa and up least to 300 GPa.

The crystal structures of novel R-3m-H_3SXe, $C2/m$-H_3SXe, P-3m1-H_3SXe and Pm-3m-H_3SXe are presented in Fig. 2. For comparison, the crystal structures of H_3S are also shown in Figs. 2(a)–(c). The low-pressure H_3SXe is predicted to take the hexagonal R-3m space group. The equilibrium lattice parameters of R-3m-H_3SXe are $a = 4.69$ Å, $b = 4.69$ Å, $c = 23.50$ Å at 90 GPa [Figs. 2(d) and (h)]. The coordination numbers of sulfur atoms are three and six in R-3m-H_3SXe. There are isolated SH_6 and SH_3 units in R-3m-H_3SXe. There is larger van der Waals volume in R-3m-H_3SXe. The S-H bond length of R-3m-H_3SXe is 1.376 and 1.412 Å and the S-H$\cdots$S distance is 1.616 Å. Different from $Cccm$-H_3S where the H_2 dimers are observed in its crystal structure, all the hydrogen atoms form covalent bonds with their neighboring sulfur atoms in R-3m-H_3SXe. The presence of Xe help the H-H bonds of H_2 break. At 90 GPa, the R-3m phase transforms to $C2/m$-H_3SXe. The $C2/m$-H_3SXe has monoclinic space group $C2/m$. The equilibrium lattice parameters of $C2/m$-H_3SXe are $a = 7.75$ Å, $b = 4.47$ Å, $c = 9.48$ Å, $\beta = 144.8°$ at 140 GPa [Figs. 2(e) and (i)].

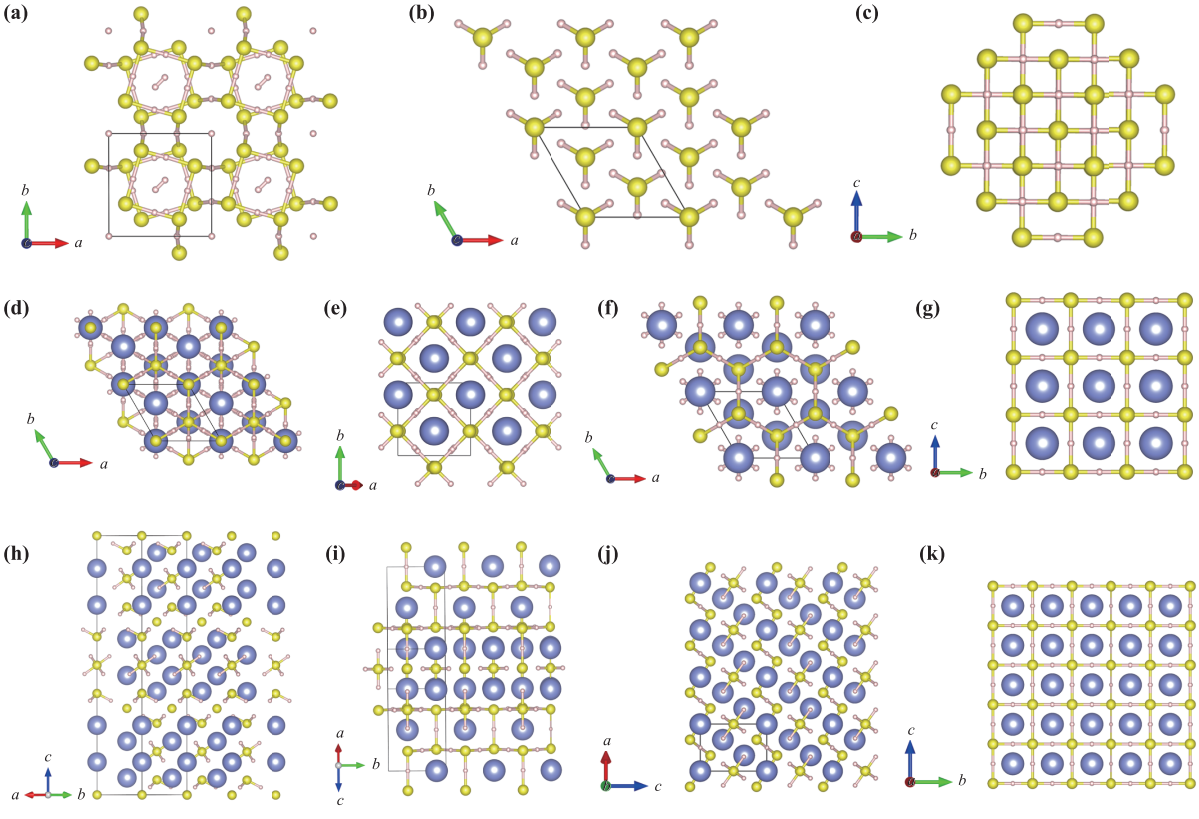

Fig. 2 The crystal structures of H_3S with **(a)** $Cccm$ **(b)** $R3m$ **(c)** Im-3m space groups. And the crystal structures of H_3SXe with R-3m **(d, h)**, $C2/m$ **(e, i)**, P-3m1 **(f, j)**, and Pm-3m **(g, k)** space groups. The blue, yellow, and pink spheres denote Xe, S and H atoms, respectively.

The coordination numbers of sulfur atoms are three and six in $C2/m$-H_3SXe. The partial hydrogen-bond symmetrization is formed in $C2/m$-H_3SXe. In addition to the hydrogen-bond symmetrized S–H–S, there are also isolated SH_6 units in $C2/m$-H_3SXe. P-$3m1$-H_3SXe crystallizes with hexagonal P-$3m1$ space group [Figs. 2(f) and (j)]. At 200 GPa, the equilibrium lattice parameters are a = 4.31 Å, b = 4.31 Å, and c = 5.27 Å. Within this structure, six inequivalent atoms occupy the crystallographic 6i (H: 0.156, 0.311, 0.342), 3e (H: 0.5, 0.5, 0), 2d (S: 0.667, 0.333, 0.842), 1b (S: 0, 0, 0.5), 2d (Xe: 0.667, 0.333, 0.338) and 1a (Xe: 0, 0, 0) positions in the unit cell. The P-$3m1$-H_3SXe is closely related to the $R3m$-H_3S. The 'H_3S' host lattice of P-$3m1$-H_3SXe is very similar to the framework of $R3m$-H_3S. The coordination numbers of sulfur atoms are three and six. One can observe graphene-like array formed together by S and H atoms, parallel to the ab plane. The partial hydrogen-bond symmetrization appears in P-$3m1$-H_3SXe. Furthermore, there are isolated SH_6 units in P-$3m1$-H_3SXe. The S-H bond lengths of P-$3m1$-H_3SXe are 1.430 Å and 1.496 Å. The distance of H-S$\cdots$H is 1.641 Å at 200 GPa. Partial S-H bond lengths are smaller than that of Im-$3m$ H_3S (1.493 Å) at 200 GPa, indicating that there are much stronger hydrogen–sulfur interatomic interactions in P-$3m1$-H_3SXe than that in Im-$3m$-H_3S. The H-S-H bond angles are 89.58°, 89.44°, 90.56°, and 92.06° which are very close to that of Im-$3m$-H_3S (90°). The presence of isolated SH_6 units will decrease the number of free electrons in P-$3m1$-H_3SXe, resulting the decrease of metallicity. High-pressure Pm-3m-H_3SXe crystallizes with cubic Pm-$3m$ space group [Figs. 2(g) and (k)]. At 240 GPa, the equilibrium lattice parameters are a = 2.98 Å. Within this structure, six inequivalent atoms occupy the crystallographic 3d (H: 0.5, 0.0, 0.0), 1a (S: 0.0, 0.0, 0.0) and 1b (Xe: 0.5, 0.5, 0.5) positions in the unit cell. The Pm-$3m$-H_3SXe is closely related to the Im-$3m$-H_3S. Pm-$3m$-H_3SXe can be obtained by replacing the partial SH_6 octahedron of Im-$3m$-H_3S with Xe atoms. Pm-$3m$-H_3SXe has the same S–H framework as that of Im-$3m$-H_3S (Fig. S3). The sulfur atoms in Pm-$3m$-H_3SXe has the same coordination number (six) as that of Im-$3m$-H_3S. The complete hydrogen-bond symmetrization is formed in Pm-$3m$-H_3SXe. The S–H bond lengths of Pm-$3m$-H_3SXe are 1.49 Å, which is larger than that of Im-$3m$-H_3S (1.47 Å) at 240 GPa. Obvious lattice expansion can be found in the crystal structure of Pm-$3m$-H_3SXe. Furthermore, these results suggest good hydrogen-bond symmetrization feature induced by doped Xe in H_3SXe. Under compression, the hydrogen bond symmetrization of H_3SXe enhances, accompanied by the R-$3m$ $\rightarrow$ $C2/m$ $\rightarrow$ P-$3m1$ and further to Pm-$3m$ structural phase transitions.

In order to understand the structural stability and bonding mechanisms of H_3SXe, the electron localization function (ELF) of R-$3m$-H_3SXe, $C2/m$-H_3SXe, P-$3m1$-H_3SXe, and Pm-$3m$-H_3SXe in the specific planes have been calculated. Figure 3 shows large areas with big ELF values (approximately 0.85) between S and H atoms in these four H_3SXe phases, which are typical of strong covalent bonding. The ELF isosurfaces clearly illustrate the presence of 6-fold coordinated sulfur atoms in R-3m-H_3SXe and $C2/m$-H_3SXe (Fig. S4). There are lone pair electrons in hydrogen atoms of partial S–H bonds,

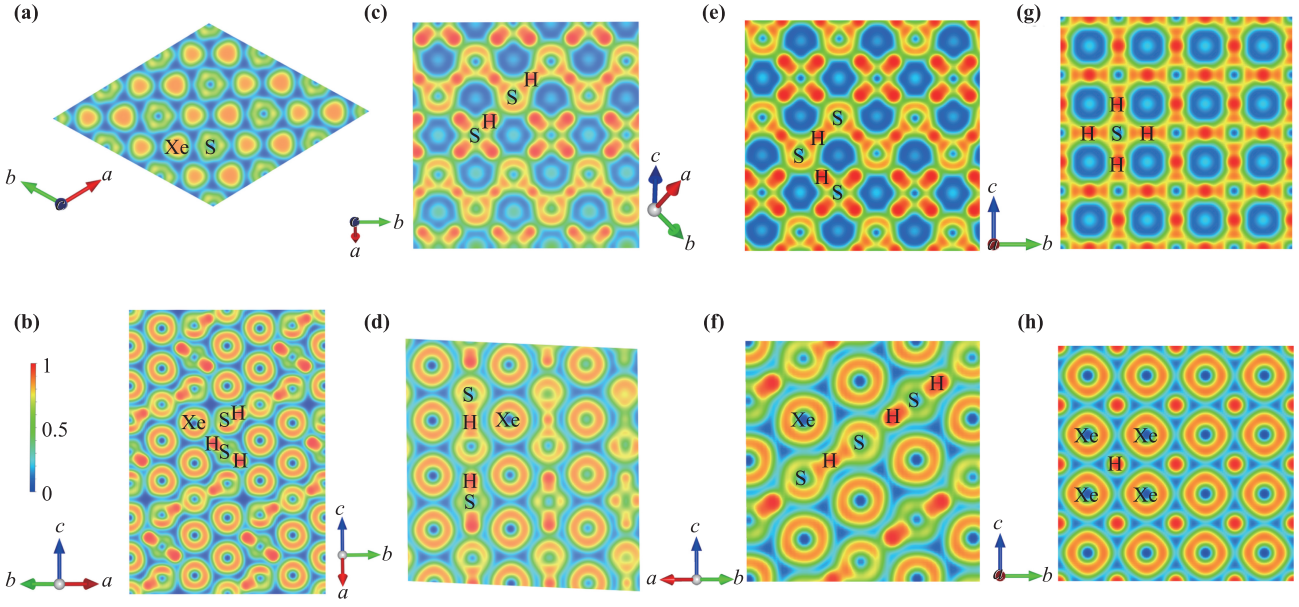

Fig. 3 The 2D electron localization function slice of R-3m-H_3SXe **(a, b)**, $C2/m$-H_3SXe **(c, d)**, P-$3m1$-H_3SXe **(e, f)** and Pm-$3m$-H_3SXe **(g, h)**.

indicating the presence of molecule-like units. Obvious partial hydrogen-bond symmetrization feature have been observed in R-3m-H_3SXe and $C2/m$-H_3SXe [Figs. 3(a)–(d)]. The high pressure makes the hydrogen-bond symmetrization enhance as shown in Fig. 3e and 3f. Then the partial hydrogen-bond symmetrization transforms to the complete hydrogen-bond symmetrization as shown in Figs. 3(g) and (h). In Pm-3m-H_3SXe, the hydrogen-bond symmetrization progress is finished. The hydrogen atoms are located in the middle of symmetrical S–H–S bonding [Fig. 3(g)]. Furthermore, the ELF results also indicate that there is no covalent bonding between Xe and H/S atoms. There is repulsive interaction between Xe atoms and 'H_3S' host lattice, which induces the lattice expansion in H_3SXe.

In order to investigate the effect of the chemical precompression induced by Xe atoms, we studied the electronic band structure and density of state of H_3SXe and compared them with that of H_3S at their stable pressures. The R-3m-H_3SXe is an insulator with the band gap of 1.52 eV. In R-3m-H_3SXe, there are no H_2 dimers in its crystal structure; all the hydrogen atoms form covalent bonds with their neighboring sulfur atoms. In addition to the large van der Waals volume, these covalent bonds are responsible for the insulating properties because there are little free electrons in R-3m-H_3SXe. Furthermore, the presence of Xe atoms induce the lattice expansion in Xe–H_3S system. So it is found that the band gap of R-3m-H_3SXe is larger than that of $Cccm$-H_3S (0.49 eV). The other phases of H_3SXe are metallic because of the finite DOS at the Fermi level (E_f) as shown in Fig. 4. For the case of $C2/m$-H_3SXe, it is found that many bands cross the Fermi level along the Z → Y, Y → B, and B → E directions in the electronic band structure. These bands are mainly composed of H_1s, S_3p and Xe_5p orbitals. In $C2/m$-H_3SXe, there are also no H_2 dimers in its crystal structure, all the hydrogen atoms form covalent bonds with their neighboring sulfur atoms. And obvious hydrogen-bond symmetrization feature can be found in the ELF of $C2/m$-H_3SXe. These are responsible for the formation of bands crossing the fermi level. The DOS indicates that the Xe_5p electrons contribute the metallicity of $C2/m$-H_3SXe. For the case of P-3m1-H_3SXe, the strong hybridization between H_s and S_p orbitals are found. Note that many bands crossing the Fermi level, which lead to a larger electronic DOS at the Fermi level. The electronic density of states (DOS) near the Fermi level is dominated by the H_1s, S_3p and

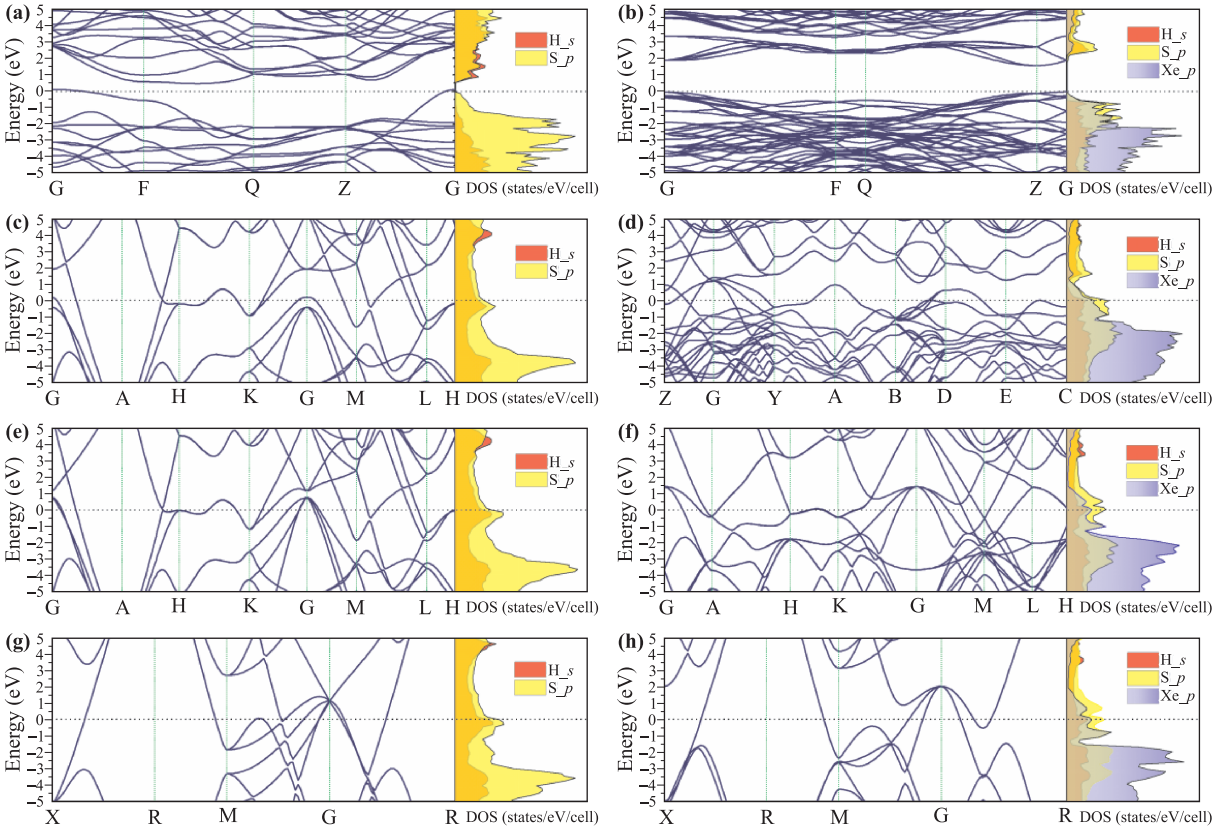

Fig. 4 The electronic band structure and density of states of H_3S and H_3SXe. **(a)** $Cccm$-H_3S and **(b)** R-3m-H_3SXe at 90 GPa, **(c)** $R3m$-H_3S and **(d)** $C2/m$-H_3SXe at 140 GPa, **(e)** $R3m$-H_3S and **(f)** P-3m1-H_3SXe at 180 GPa, **(g)** Im-3m-H_3S and **(h)** Pm-3m-H_3SXe at 240 GPa.

Xe_5p states. The Xe atoms can affect the metallicity of P-3m1-H_3SXe. The DOS of Pm-3m-H_3SXe at 220 GPa suggests that it is a good metallic material. Similar to Im-3m-H_3S, obvious strong orbital hybridization between the H_1s and S_3p orbitals are found. Note that many bands crossing the Fermi level, which lead to a larger electronic DOS N_{ef} at the Fermi level. The density of states at the fermi level are mainly originated from the H_1s, S_3p and Xe_5p states. Furthermore, in addition to similar structural parameters, Pm-3m-H_3SXe has similar electronic band structure and density of states around the Fermi level as that of Im-3m-H_3S as shown in Figs. 4(g) and (h). The larger N_{ef} of Pm-3m-H_3SXe could contribute to a higher T_c. So Pm-3m-H_3SXe can be expected as the most potential superconducting phase in H_3SXe.

We now discuss the superconductivity of Pm-3m-H_3SXe. The calculated Eliashberg phonon spectral function $\alpha^2F(\omega)$ and the integrated EPC parameter λ of Pm-3m-H_3SXe at 240 GPa are shown in Fig. 5(a). The calculated EPC parameter λ is 1.16, indicating that the EPC of Pm-3m-H_3SXe is very strong. The phonon frequency logarithmic average ω_{log} calculated directly from the phonon spectrum is 1176 K. The standard effective Coulomb repulsion parameter μ^* value of 0.13 is used to estimate the critical temperature T_c of Pm-3m-H_3SXe. Base on the Allen-Dynes modified McMillan equation, the estimated T_c of Pm-3m-H_3SXe is 89 K which is larger than that of the famous MgB_2, but is much smaller than that of our previously predicted Im-3m-H_3S ($\lambda = 2.19$, $T_c = 200$ K at 200 GPa). From the phonon density of Pm-3m-H_3SXe, it is found that the acoustic phonon modes come from the Xe atoms as expected. Compare to the projected phonon DOS, it is found that the acoustic mode of Pm-3m-H_3SXe, mainly contributed by the vibration of Xe atoms, constitutes 14% of the total λ. The optical modes composed of the vibration of S atoms constitutes 23% of the total λ. The remaining parts of the λ (63% of the total λ) are mainly derived from the optical mode which is all attributed by the vibration of the H atoms. So the vibration of "H_3S" host lattice mainly contributes the superconductivity of Pm-3m-H_3SXe. Previous high-pressure study already suggests that the EPC intensity of Xe is very low. The maximum critical temperature of Xe is only 0.04 K at 215 GPa [58]. So the superconducting properties of Xe have little influence for the reduction of the superconductivity in Pm-3m-H_3SXe. From the projected EPC parameter λ, it is found that the soft phonon modes, especially in the phonon branch 3 (the vibration of Xe atoms), 4 (the vibration of S atoms) and 7 (the vibration of H atoms) are responsible for the EPC parameter λ. The phonon branch 7 is the most important mode for the H atoms vibration. Almost all the contribution of H vibration for the λ comes from the phonon branch 7. In the $R \to \Gamma \to M$ directions, especially the $R \to \Gamma$ direction, the phonon mode softening of the phonon branch 7 is resonant with that of the phonon branch 3 and branch 4, indicating that although the vibration of "H_3S" host lattice mainly contribute the superconductivity of Pm-3m-H_3SXe, the guest lattice (Xe atoms) has the ability to affect the EPC of "H_3S" host lattice. Meanwhile, it is found that the presence of Xe only induces the lattice expansion of Pm-3m-H_3SXe with reference to Im-3m-H_3S.

In order to study the effect of atomic mass, we have constructed a hypothetical model system of Pm-3m-H_3SM (M = Ne, Ar, Kr, and Xe), in which Xe atoms of Pm-3m-H_3SXe are replaced by the Ne, Ar, and Kr atoms. The phonon calculations indicate that the Pm-3m-H_3SNe is not dynamically stable at 240 GPa (Fig. 6).

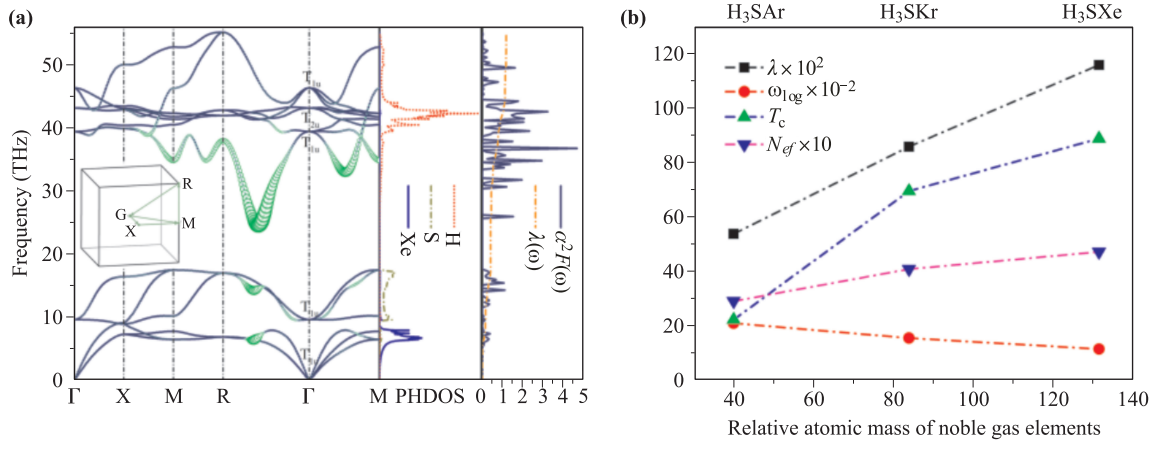

Fig. 5 **(a)** Phonon dispersion curves, phonon density of states projected on the H, S, and Xe, and the Eliashberg spectral function $\alpha^2F(\omega)$ together with the electron-phonon integral λ for Pm-3m-H_3SXe at 240 GPa. The green circles projected on phonon dispersion curves show the electron-phonon coupling and sizes of circles are proportional to the EPC strength. **(b)** The evolution of λ, ω_{log}, N_{ef}, and T_c of H_3SM (M= Ar, Kr, and Xe) at 240 GPa with respect to relative atomic mass.

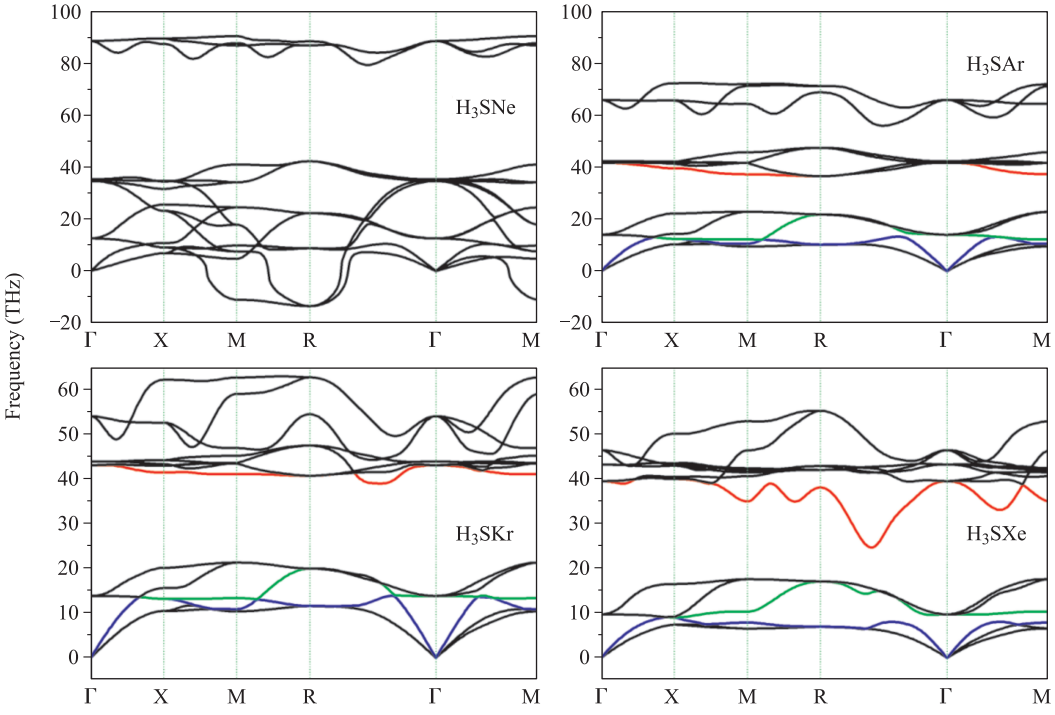

Fig. 6 The evolution of phonon dispersion of H_3SM (M = Ne, Ar, Kr, and Xe).

The *Pm*-3*m*-H_3SAr and *Pm*-3*m*-H_3SKr are stable at 240 GPa. We studied the superconductivity of this hypothetical model. With increasing relative atomic mass, we find an almost linear increase of the λ in H_3SM [Fig. 5(b)]. The T_c and N_{ef} have similar trends with that of λ. The *Pm*-3*m*-H_3SAr has the smallest T_c value of 22 K. However, the ω_{log} decreases with the relative atomic mass increasing. Considering the Allen–Dynes modified McMillan equation, T_c is a balanced result of two key parameters λ and ω_{log}. The increased trend of T_c indicates that the λ dominates the superconductivity of H_3SM. Furthermore, Fig. 6 indicates that with the relative atomic mass increasing, the phonon frequency of the different vibrational modes decreases. Interestingly, with the relative atomic mass increasing, there are softened modes in H_3SM (X = Ar, Kr, and Xe). The phonon branch 7 (red line) tends to soften. In the *Pm*-3*m*-H_3SXe, there are the most softened phonon modes because the heaviest Xe atoms will induce the biggest lattice expansion in H_3SM (Ar, Kr, Xe) system. Meanwhile, the crystal structure of H_3SM (Ar, Kr, Xe) becomes unstable. This will aggravate the softening of phonon branch 7. Moreover, it is found that the softening of the phonon branch 7 is resonant with that of the phonon branch 3 and branch 4 (blue and green lines), accompanied by the increase of the T_c values. So H_3SM is a typical phonon-mediated high-temperature superconductor. We can expect that the H_3SRn has higher superconducting critical temperature.

4 Conclusions

In summary, we explore the high-pressure phases and superconductivity of the novel H_3S–Xe compounds by using *ab initio* calculations. A novel ternary compound H_3SXe become thermodynamically stable with respect to decomposition into the H_3S and Xe. Three high-pressure structural phase transitions (*R*-3*m*-H_3SXe → *C*2/*m*-H_3SXe → *P*-3*m*1-H_3SXe → *Pm*-3*m*-H_3SXe) have been predicted at 90, 160 and 220 GPa, respectively. With increasing the pressures, the partial hydrogen-bond symmetrization transforms to the complete hydrogen-bond symmetrization in H_3SXe, accompanied by the structural phase transitions. The main structural features of the famous *Im*-3*m*-H_3S are preserved in our predicted *Pm*-3*m*-H_3SXe. The *Pm*-3*m*-H_3SXe is a potential high-temperature superconductor with a T_c value of 89 K at 240 GPa. The "H_3S" host lattice of *Pm*-3*m*-H_3SXe plays a crucial role in influencing the T_c value. Although the presence of Xe atoms do not enhance the superconductivity of H_3S, Xe atoms have the capability of accelerating the hydrogen-bond symmetrization in H_3SXe. Furthermore, the atomic mass of the noble gas elements is very important for the phonon-medicated superconductivity.

Acknowledgements This work was supported by the National Natural Science Foundation of China (Grant Nos. 11404134, 91745203, 51572108, 11634004, 11574109, and 11674122), Program

for Changjiang Scholars and Innovative Research Team in University (No. IRT_15R23), National Fund for Fostering Talents of Basic Science (No. J1103202), Jilin Provincial Science and Technology Development Project of China (Grant Nos. 20160520016JH and 20170520116JH) and China Postdoctoral Science Foundation (Grant Nos. 2014M561279 and 2016T90246). Parts of calculations were performed in the High Performance Computing Center (HPCC) of Jilin University.

References

1. I. I. Mazin, Superconductivity: Extraordinarily conventional, *Nature* 525(7567), 40 (2015)
2. I. Božović A conventional conundrum, *Nat. Phys.* 12(1), 22 (2016)
3. A. P. Drozdov, M. I. Eremets, I. A. Troyan, V. Ksenofontov, and S. I. Shylin, Conventional superconductivity at 203 kelvin at high pressures in the sulfur hydride system, *Nature* 525(7567), 73 (2015)
4. M. Einaga, M. Sakata, T. Ishikawa, K. Shimizu, M. I. Eremets, A. P. Drozdov, I. A. Troyan, N. Hirao, and Y. Ohishi, Crystal structure of the superconducting phase of sulfur hydride, *Nat. Phys.* 12(9), 835 (2016)
5. D. Duan, Y. Liu, F. Tian, D. Li, X. Huang, Z. Zhao, H. Yu, B. Liu, W. Tian, and T. Cui, Pressure-induced metallization of dense $(H_2S)_2H_2$ with high-T_c superconductivity, *Sci. Rep.* 4(1), 6968 (2015)
6. L. Ortenzi, E. Cappelluti, and L. Pietronero, Band structure and electron-phonon coupling in H_3S: A tight-binding model, *Phys. Rev. B* 94(6), 064507 (2016)
7. D. A. Papaconstantopoulos, B. M. Klein, M. J. Mehl, and W. E. Pickett, Cubic H_3S around 200 GPa: An atomic hydrogen superconductor stabilized by sulfur, *Phys. Rev. B* 91(18), 184511 (2015)
8. N. Bernstein, C. S. Hellberg, M. D. Johannes, I. I. Mazin, and M. J. Mehl, What superconducts in sulfur hydrides under pressure and why, *Phys. Rev. B* 91(6), 060511 (2015)
9. A. Bianconi and T. Jarlborg, Superconductivity above the lowest Earth temperature in pressurized sulfur hydride, *EPL* 112(3), 37001 (2015)
10. Y. Quan and W. E. Pickett, Van Hove singularities and spectral smearing in high-temperature superconducting H_3S, *Phys. Rev. B* 93(10), 104526 (2016)
11. A. F. Goncharov, S. S. Lobanov, I. Kruglov, X. M. Zhao, X. J. Chen, A. R. Oganov, Z. Konôpková, and V. B. Prakapenka, Hydrogen sulfide at high pressure: Change in stoichiometry, *Phys. Rev. B* 93(17), 174105 (2016)
12. Y. Yuan, Y. Feng, L. Bian, D.B. Zhang, and X.Z. Li, The quantum nature of the superconducting hydrogen sulfide at finite temperatures, arXiv: 1607.02348 [cond-mat] (2016)
13. A. P. Durajski, Quantitative analysis of nonadiabatic effects in dense H_3S and PH_3 superconductors, *Sci. Rep.* 6(1), 38570 (2016)
14. H. Wang, X. Li, G. Gao, Y. Li, and Y. Ma, Hydrogen-rich superconductors at high pressures, *Wiley Interdiscip. Rev. Comput. Mol. Sci.* 8(1), e1330 (2018)
15. Y. Yao and S. Tse John, Superconducting hydrogen sulfide, *Chemistry* 24(8), 1769 (2017)
16. R. Szczesniak and A. P. Durajski, The isotope effect in H_3S superconductor, *Solid State Commun.* 249, 30 (2017)
17. A. P. Durajski and R. Szczęśniak, First-principles study of superconducting hydrogen sulfide at pressure up to 500 GPa, *Sci. Rep.* 7(1), 4473 (2017)
18. S. Azadi and T. D. Kühne, High-pressure hydrogen sulfide by diffusion quantum Monte Carlo, *J. Chem. Phys.* 146(8), 084503 (2017)
19. R. Akashi, M. Kawamura, S. Tsuneyuki, Y. Nomura, and R. Arita, First-principles study of the pressure and crystal-structure dependences of the superconducting transition temperature in compressed sulfur hydrides, *Phys. Rev. B* 91(22), 224513 (2015)
20. I. Errea, M. Calandra, C. J. Pickard, J. Nelson, R. J. Needs, Y. Li, H. Liu, Y. Zhang, Y. Ma, and F. Mauri, High-pressure hydrogen sulfide from first principles: A strongly anharmonic phonon-mediated superconductor, *Phys. Rev. Lett.* 114(15), 157004 (2015)
21. C. Heil and L. Boeri, Influence of bonding on superconductivity in high-pressure hydrides, *Phys. Rev. B* 92(6), 060508 (2015)
22. Y. Ge, F. Zhang, and Y. Yao, First-principles demonstration of superconductivity at 280 K in hydrogen sulfide with low phosphorus substitution, *Phys. Rev. B* 93(22), 224513 (2016)
23. M. Komelj and H. Krakauer, Electron-phonon coupling and exchange-correlation effects in superconducting H 3 S under high pressure, *Phys. Rev. B* 92(20), 205125 (2015)
24. E. J. Nicol and J. P. Carbotte, Comparison of pressurized sulfur hydride with conventional superconductors, *Phys. Rev. B* 91(22), 220507 (2015)
25. A. F. Goncharov, S. S. Lobanov, V. B. Prakapenka, and E. Greenberg, Stable high-pressure phases in the H-S system determined by chemically reacting hydrogen and sulfur, *Phys. Rev. B* 95(14), 140101 (2017)
26. B. Guigue, A. Marizy, and P. Loubeyre, Direct synthesis of pure H_3S from S and H elements: No evidence of the cubic superconducting phase up to 160 GPa, *Phys. Rev. B* 95(2), 020104 (2017)
27. H. Wang, J. S. Tse, K. Tanaka, T. Iitaka, and Y. Ma, Superconductive sodalite-like clathrate calcium hydride at high pressures, *Proc. Natl. Acad. Sci. USA* 109(17), 6463 (2012)

28. Y. Li, L. Wang, H. Liu, Y. Zhang, J. Hao, C. J. Pickard, J. R. Nelson, R. J. Needs, W. Li, Y. Huang, I. Errea, M. Calandra, F. Mauri, and Y. Ma, Dissociation products and structures of solid H_2S at strong compression, *Phys. Rev. B* 93(2), 020103 (2016)
29. T. Ishikawa, A. Nakanishi, K. Shimizu, H. Katayama-Yoshida, T. Oda, and N. Suzuki, Superconducting H5S2 phase in sulfur-hydrogen system under high-pressure, *Sci. Rep.* 6(1), 23160 (2016)
30. A. P. Drozdov, M. I. Eremets, and I. A. Troyan, Superconductivity above 100 K in PH_3 at high pressures, arXiv: 1508.06224 [cond-mat] (2015)
31. H. Oh, S. Coh, and M. L. Cohen, Comparative study of high-Tc superconductivity in H_3S and H_3P, arXiv: 1606.09477 [cond-mat] (2016)
32. A. Shamp, T. Terpstra, T. Bi, Z. Falls, P. Avery, and E. Zurek, Decomposition Products of Phosphine Under Pressure: PH_2 Stable and Superconducting? *J. Am. Chem. Soc.* 138(6), 1884 (2016)
33. S. Zhang, Y. Wang, J. Zhang, H. Liu, X. Zhong, H. F. Song, G. Yang, L. Zhang, and Y. Ma, Phase Diagram and high-temperature superconductivity of compressed selenium hydrides, *Sci. Rep.* 5(1), 15433 (2015)
34. X. Zhong, H. Wang, J. Zhang, H. Liu, S. Zhang, H. F. Song, G. Yang, L. Zhang, and Y. Ma, Tellurium hydrides at high pressures: High-temperature superconductors, *Phys. Rev. Lett.* 116(5), 057002 (2016)
35. K. Abe and N. W. Ashcroft, Stabilization and highly metallic properties of heavy group-V hydrides at high pressures, *Phys. Rev. B* 92(22), 224109 (2015)
36. Y. Fu, et al., Chem. Mater. (2016)
37. Y. Ma, et al., The unexpected binding and superconductivity in SbH4 at high pressure, arXiv: 1506.03889 [cond-mat] (2015)
38. Y. Wang, H. Wang, J. S. Tse, T. Iitaka, and Y. Ma, Structural morphologies of high-pressure polymorphs of strontium hydrides, *Phys. Chem. Chem. Phys.* 17, 19379 (2015)
39. Y. Li, J. Hao, H. Liu, J. S. Tse, Y. Wang, and Y. Ma, Pressure-stabilized superconductive yttrium hydrides, *Sci. Rep.* 5(1), 9948 (2015)
40. M. M. D. Esfahani, Z. Wang, A. R. Oganov, H. Dong, Q. Zhu, S. Wang, M. S. Rakitin, and X. F. Zhou, Superconductivity of novel tin hydrides (Sn_nH_m) under pressure, *Sci. Rep.* 6(1), 22873 (2016)
41. H. Liu, I. I. Naumov, R. Hoffmann, N. W. Ashcroft, and R. J. Hemley, Potential high-T_c superconducting lanthanum and yttrium hydrides at high pressure, *Proc. Natl. Acad. Sci. USA* 114, 6990 (2017)
42. I. A. Kruglov, et al., Uranium polyhydrides at moderate pressures: Prediction, synthesis, and expected superconductivity, arXiv: 1708.05251 [cond-mat] (2017)
43. M. Rahm, R. Hoffmann, and N. W. Ashcroft, Ternary gold hydrides: Routes to stable and potentially superconducting compounds, *J. Am. Chem. Soc.* 139(25), 8740 (2017)
44. S. Zhang, L. Zhu, H. Liu, and G. Yang, Structure and electronic properties of Fe_2SH_3 compound under high pressure, *Inorg. Chem.* 55(21), 11434 (2016)
45. T. Muramatsu, W. K. Wanene, M. Somayazulu, E. Vinitsky, D. Chandra, T. A. Strobel, V. V. Struzhkin, and R. J. Hemley, Metallization and superconductivity in the hydrogen-rich ionic salt $BaReH_9$, *J. Phys. Chem. C* 119(32), 18007 (2015)
46. Y. Ma, D. Duan, Z. Shao, H. Yu, H. Liu, F. Tian, X. Huang, D. Li, B. Liu, and T. Cui, Divergent synthesis routes and superconductivity of ternary hydride $MgSiH_6$ at high pressure, *Phys. Rev. B* 96(14), 144518 (2017)
47. Y. Ma, D. Duan, Z. Shao, D. Li, L. Wang, H. Yu, F. Tian, H. Xie, B. Liu, and T. Cui, Prediction of superconducting ternary hydride $MgGeH_6$: From divergent high-pressure formation routes, *Phys. Chem. Chem. Phys.* 19(40), 27406 (2017)
48. W. Kohn and L. J. Sham, Self-consistent equations including exchange and correlation effects, *Phys. Rev.* 140(4A), A1133 (1965)
49. P. Hohenberg and W. Kohn, Inhomogeneous electron gas, *Phys. Rev.* 136(3B), B864 (1964)
50. G. Kresse and D. Joubert, From ultrasoft pseudopotentials to the projector augmented-wave method, *Phys. Rev. B* 59(3), 1758 (1999)
51. G. Kresse and J. Furthmüller, Efficient iterative schemes for *ab initio* total-energy calculations using a plane-wave basis set, *Phys. Rev. B* 54(16), 11169 (1996)
52. P. E. Blöchl, Projector augmented-wave method, *Phys. Rev. B* 50(24), 17953 (1994)
53. J. P. Perdew, K. Burke, and M. Ernzerhof, Generalized gradient approximation made simple, *Phys. Rev. Lett.* 77(18), 3865 (1996)
54. A. Togo, F. Oba, and I. Tanaka, First-principles calculations of the ferroelastic transition between rutile-type and $CaCl_2$-type SiO_2 at high pressures, *Phys. Rev. B* 78(13), 134106 (2008)
55. P. Giannozzi, S. Baroni, N. Bonini, M. Calandra, R. Car, et al., QUANTUM ESPRESSO: A modular and open-source software project for quantum simulations of materials, *J. Phys.: Condens. Matter* 21(39), 395502 (2009)
56. Y. Wang, J. Lv, L. Zhu, and Y. Ma, CALYPSO: A method for crystal structure prediction, *Comput. Phys. Commun.* 183(10), 2063 (2012)
57. Y. Wang, J. Lv, L. Zhu, and Y. Ma, Crystal structure prediction via particle-swarm optimization, *Phys. Rev. B* 82(9), 094116 (2010)
58. Y. Yao and J. S. Tse, Electron-phonon coupling in the high-pressure hcp phase of xenon: A first-principles study, *Phys. Rev. B* 75(13), 134104 (2007)